



WAVELENGTH AND AMPLITUDE MEASUREMENT OF AN UNSTABLE WAKE VORTEX BENDING MODE VIA HELIUM-BUBBLE VISUALIZATION

Brian M. Babie, Robert C. Nelson
University of Notre Dame, Notre Dame, IN 46556, USA

KEYWORDS:

Main subject(s): *wake vortex stability*

Fluid: *air*

Visualization method(s): *helium-bubble injection*

Other keywords: *trailing vortices, Crow instability, helium-bubble injection*

ABSTRACT : *This paper describes a research study that examines the potential of exciting instability modes in a trailing vortex wake to cause the premature breakup and decay of these hazardous wake structures. A four-vortex model has been selected for this study as it is representative of a landing aircraft wake; a flight stage that is most prone to wake encounters. Previous work done by the authors has resulted in the identification of a region of counter-rotating wake configurations that are conducive to large temporal instability growth rates. This region is also observed to include those configurations which are known to translate rigidly. The driving hypothesis of the current work is that the observed unstable motion is a long-wavelength instability that is driven by the mutual interaction of the tip/flap vortex pair on each side of the wake centerline. The helium-bubble visualization technique has been used as an effective tool for the identification of the long-wavelength instability. The data attained from visual images of the wake have been used to obtain quantitative estimates of the bending mode wavelength and amplitude for comparison with linear stability theory.*

1 Introduction to the Study of Aircraft Wakes

Most major airports operate near capacity during peak operating times. Although new technology has been developed that would allow for increases in airport traffic, they can not be utilized until the hazard posed by aircraft trailing vortex wakes has been mitigated. Viscous diffusion of trailing vortex wakes in calm atmospheric conditions simply takes too long. However, trailing vortex wakes are known to exhibit certain instability modes that, if excited, result in the rapid breakup and decay of the wake.

The focus of this research program was to examine these wake instability modes both analytically and experimentally. The primary objective was to investigate trailing vortex wake configurations under controlled conditions of wake geometry and circulation strength to gain additional insight into the flow physics of these instability modes. While the study included detailed flow surveys through the wake, the current paper will focus on the use of flow visualization to observe wake instabilities and the use of digital images to provide quantitative information on instability growth rate and wavelength as a function of the controlled parameters.

1.1 Why Use a Four-Vortex Model?

A unique experimental set-up was developed to simulate the trailing wake structure behind commercial jet aircraft during take-off and landing. When flaps are deployed, a typical aircraft wake consists of multiple vortex pairs. A four-vortex model has been shown to provide an acceptable model for the study of high-lift aircraft wakes [1]. To study a four-vortex wake, a series of four half-span models were used to create four wake vortices, with the vortex span and circulation strength being controlled by the lateral spacing and the angle of attack of the wing models, respectively. Figure 1 shows the arrangement of the wake generating device. This experimental set-up enabled the investigation of the far-field wake dynamics that were not restricted to a single spanwise loading condition, such as that resulting from the use of an airplane model. Effectively, the experimental apparatus permits the study of complex wake geometries that are entirely under the control of the researcher.

1.2 The Long-Wavelength Instability

The instability mode that becomes of primary interest for the current study of aircraft wakes is a long-wavelength bending mode, of which the well-known Crow instability [2] represents a specific case. The long-wavelength instability is manifested in the form of a radial displacement of the entire vortex core and resembles a periodic wave in the axial direction. The amplification of the bending mode is driven by the mutual interaction of the vortices within the pair, such that symmetric waves tend to grow on both vortices within the pair. It is also critical to note that the growth rate of the bending wave scales with the applied strain rate (ε), where $\varepsilon_i = \Gamma_j / 2\pi b^2$, such that the wave will grow faster with increases in circulation strength (Γ) and reductions in the lateral spacing (b). Further, the wavelength of this particular mode is seen to scale with the vortex span, or the lateral distance between the unperturbed vortex pair.

In order to positively identify the long-wavelength instability under experimental circumstances, a code has been developed to predict the wavelength and amplitude characteristics of the anticipated instability for a given set of experimental conditions. The predictive method is based on the classic linear eigenvalue problem posed by Crow [2], where the temporal growth rate (σ) is calculated over a band of unstable axial wavenumbers. The linear stability model further includes the self-induced rotation model of Saffman [3] that is shown to be valid at all axial wavenumbers. Additionally, the model follows the technique set forth by Bristol *et al* [4] for the inclusion of parallel vortices of differing circulation strength. Ortega [5] has used an identical method to predict instabilities in the wake of a triangular-flapped wing and concluded that the two-vortex linear stability model is suitable for use in such a four-vortex system.

2 Experimental Methods

2.1 The Generic Four-Vortex Wake Model

In order to complete a study of the flow physics underlying the unstable motion of wake vortices whose results are applicable to a wide array of aircraft configurations, it was necessary to develop an experimental model capable of producing a generic four-vortex wake. To accomplish this objective, an experimental set-up consisting of four identical, independently controlled wing models was created. The wake generating apparatus is set up as a lateral cascade of four rectangular wing models molded from black epoxy. Each model consists of a NACA 0015 airfoil cross section with a $c = 5$ inch (127

mm) chord length. The models measure $b = 20$ inches (508 mm) from root to tip, where the wing tips have been rounded to a diameter equal to the thickness of the airfoil cross section. The rounded wing tips have been added to the models to eliminate a secondary vortex that is commonly observed in flows about square wing tips [6]. It is also noted that these semispan models have an aspect ratio of $AR = 8$, consistent with transport aircraft wings.

The outboard wings on the experimental set up are set at a fixed location with a span of $b_1 = 20$ inches (508 mm) between the models. The inboard wing models are mounted through a slot that is 12 inches (305 mm) in length such that in the inboard wings may be easily moved, effectively changing the flap vortex span (b_2). All four of the wing models are mounted through the floor of the leading module of the test section via stepper motor, which allows the user control over the angle of attack of each wing. With the user having control over the angle of attack of each wing model, the experimental apparatus essentially allows the user to maintain control over the circulation strength of each vortex within the flow field. A diagram of the experimental set-up is given as Figure 1. Additional information regarding the experimental set-up may be found in Babie and Nelson [7-9]. Noting that the test section of the wind tunnel measures 50 ft (15.24 m), there are nearly 30 tip vortex spans ($x/b_1 = 30$) within the test section to observe the behavior of the wake flow.

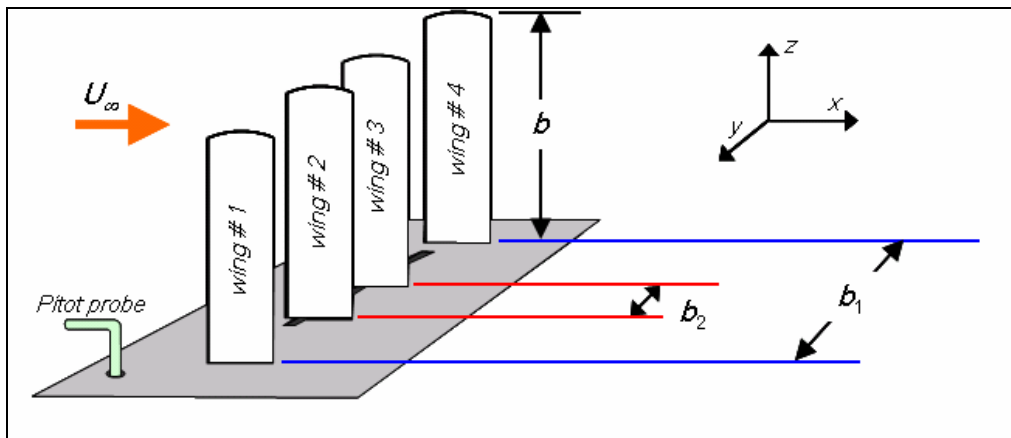


Fig. 1. Generic four-vortex wake experimental set-up at the University of Notre Dame

2.2 The Helium-Bubble Flow Visualization Technique

Because a non-intrusive flow diagnostic technique was required to study the stability of four-vortex wakes, the use of flow visualization was ideal for this study. In order to successfully view the four-vortex wake flow, a helium bubble visualization technique was used. Further examples of the use of the helium bubble visualization technique for wake vortex flows may be found in Hale *et al* [10] and Eliason *et al* [11].

To complete the flow visualization portion of this study, a Sage Action Model 5 Helium Bubble Generator was used to produce a consistent stream of neutrally buoyant bubbles that were successively injected into the flow field to seed the experimentally generated vortex cores. The Model 5 generator produces neutrally buoyant helium bubbles by injecting compressed helium into a steady stream of Sage Action 1035 Bubble Film Solution (BFS). Helium bubbles are generated inside an element of the Model 5 generator known as the plug-in head, which consists of three concentric stainless steel tubes

for the delivery of helium, BFS and compressed air into a centripetal filter. The three concentric outlet tubes on the plug-in head connect to the mini-vortex filter, such that the compressed air drives the helium/BFS/air mixture azimuthally about the filter cylinder creating a vortex flow. As a result of the swirling flow within the cylinder, only the neutrally-buoyant bubbles are driven through a stainless steel tube for delivery into the test flow while the non-neutrally-buoyant bubbles are burst on the filter walls. Each bubble head is capable of generating 400 bubbles per second, with the bubbles ranging in size from 0.05 inches (1.27 mm) to 0.15 inches (3.81 mm) in diameter.

The helium bubbles are delivered into the test flow through a 15 ft (4.57 m) length of 0.375 inch (9.53 mm) inner diameter vinyl tubing. The test section end of the delivery tubing is connected to a 4 inch (101.6 mm) length of 0.375 inch (9.53 mm) outer diameter rigid plastic tube, located 22 inches (0.559 m) upstream of the leading edge of the wing models. The bubbles are convected downstream by the free-stream flow and over the wing tip section of each model, for entrainment into the vortex core. The bubbles are illuminated using a 300 watt tungsten-halogen lamp located near the end of the test section, which contains an adjustable aperture for control of the size and shape of the illuminated field.

Helium bubbles that become entrained into the vortex cores tend to remain in the core region for the entire length of the test section. The life span of a helium bubble is on the order of one minute, with the time required for a bubble to convect the length of test section near 3 seconds. A photograph of the near-field roll-up of a single wake vortex is provided as Figure 2.

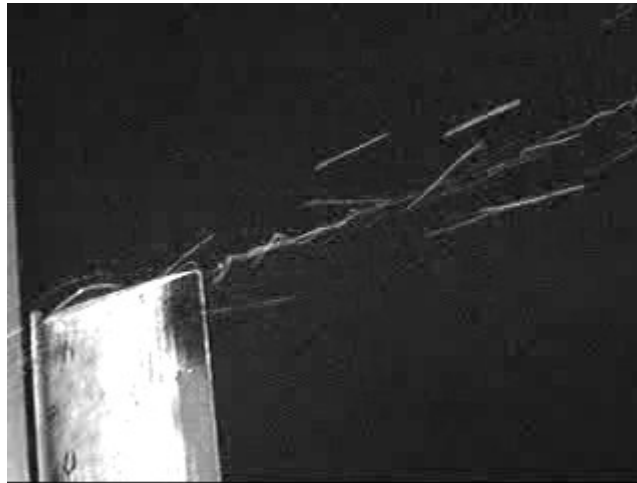


Fig. 2. Entrainment of neutrally-buoyant helium bubbles into a single vortex core

2.3 Wavelength and Amplitude Measurement Methodology

Images of the seeded and illuminated wake flow are captured by both digital photography and videography, with the camera typically located five tip-spans ($5b_1$) downstream of the measurement plane and on the far side of the wind tunnel. Using this set-up ensured that several periods of the bending motion would be observed in the camera's viewing window, while maintaining the capacity to derive wavelength and amplitude measurements. To attain a quantitative estimate of the wavelength and amplitude of these bending modes, a calibration photograph was first taken of a length reference scale using the identical camera settings that would be used in the experiment. The calibration plate measured 40 inches (1.02 m) by 20 inches (0.508 m) and consisted of a uniform grid of fiducial points,

WAVELENGTH AND AMPLITUDE MEASUREMENT OF AN UNSTABLE WAKE VORTEX BENDING MODE VIA HELIUM-BUBBLE VISUALIZATION

spaced 1.188 inches (30.18 mm) apart in both the vertical and horizontal directions. Consequently, the uncertainty of the wavelength and amplitude estimations is acknowledged to be $\delta = \pm 0.594$ inches (15.09 mm). To calibrate the video camera, the plate was placed at the desired streamwise coordinate such that the plate would represent an xz -plane intersecting the illuminated wake vortex. A still image was extracted from the calibration video and imported into Matlab, where an xz -grid was applied. A sample calibration image appears on the left side of Figure 3.

Digital video was acquired of both the inboard and outboard wake vortices at streamwise locations of $x/b_1 = 5, 10, 15$ and 20 . The circulation strength ratio was varied in the range $-0.90 \leq \Gamma_2/\Gamma_1 \leq 0$. The span ratio was maintained at $b_2/b_1 = 0.45$ throughout this entire portion of the flow visualization study. A series of still images was extracted from each video and imported into Matlab for evaluation. Matlab interprets digital images as three matrices of identical size, with the three matrices denoting the red, green and blue color intensities of a given image. Each element in a particular matrix is representative of the red, green or blue color intensity of a specific pixel in the digital image. Consequently, it was possible to replace the matrix representing the red intensities in the flow visualization image with the analogous red color matrix from the corresponding calibration image. This results in a superimposition of the flow visualization and calibration images, such that the fiducial marks on the calibration images could be used to directly estimate the wavelength and amplitude, as presented on the right side of Figure 3. The calibration plate has also been highlighted on both images to assist in the estimation of the desired linear measurements.

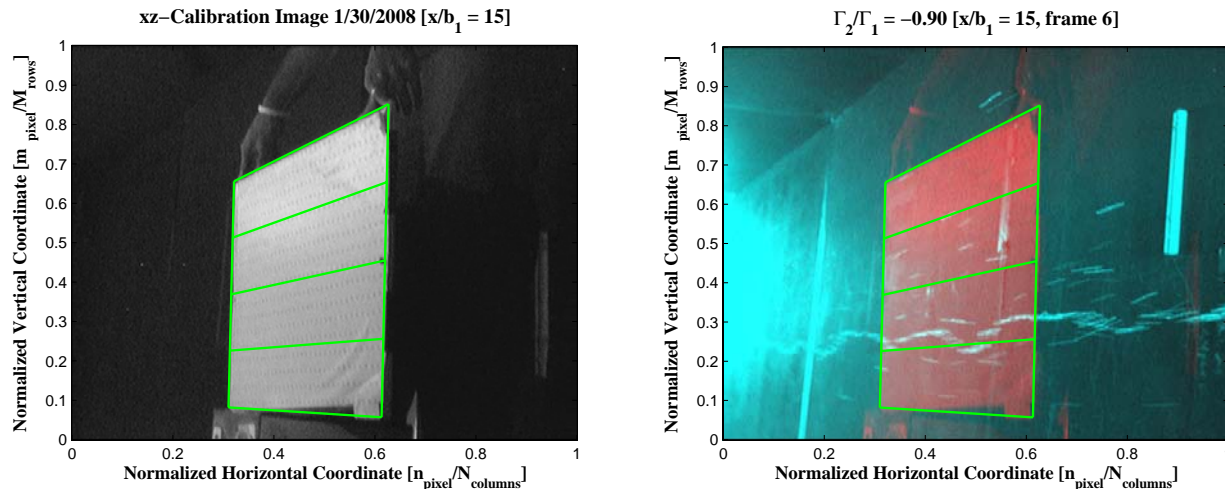


Fig. 3. Sample xz -plane calibration image (left) and a superimposition of calibration and helium-bubble flow visualization images used to estimate wavelength and amplitude (right)

In order to derive a wavelength and amplitude measurement for comparison with the linear stability theory, a series of 10 images was taken from each video. The wavelength and amplitude were estimated on each image and the mean value of each parameter was subsequently calculated.

3 Results of the Flow Visualization Experiments

3.1 Investigation of the Observed Wavelength

Consistent with the method that was prescribed in section 2.3, a series of digital videos were captured from which a group of still images was extracted for analysis. Temporal growth rates were calculated using the linear stability model with the lateral span between the inboard and outboard vortices on one side of the wake centerline as the normalizing length scale. A comparison of the predicted and measured wavelengths shows an acceptable agreement with the linear stability model for a rigidly translating system, as shown in Figure 4. The blue arched curve represents the instability growth rate over a band of wavenumbers for the particular configuration. The least stable wavenumber is denoted by the peak of the predicted curve and consequently represents the wavelength that is expected to be dominant in the observable flow field. The vertical lines in Figure 4 designate the mean wavelength measurements at several streamwise locations within the wake.

Inspection of the $\Gamma_2/\Gamma_1 = -0.90$ results in Figure 4 shows a set of measured wavelengths within the band of unstable wavenumbers, although at a slightly larger wavenumber than the peak value. This discrepancy may be attributed to several sources, including the uncertainty associated with the wavelength measurement technique and the uncertainty in the determination of the effective core radius used in the predictive solution. It is also noted that an error of 10% in the determination of the core radius would yield a 2% shift in the location of the peak growth rate. The core radius value used for the calculations presented in Figure 4 was obtained by fitting a Lamb-Oseen azimuthal velocity profile to multiple sets of hot-wire data obtained during an earlier portion of this research program.

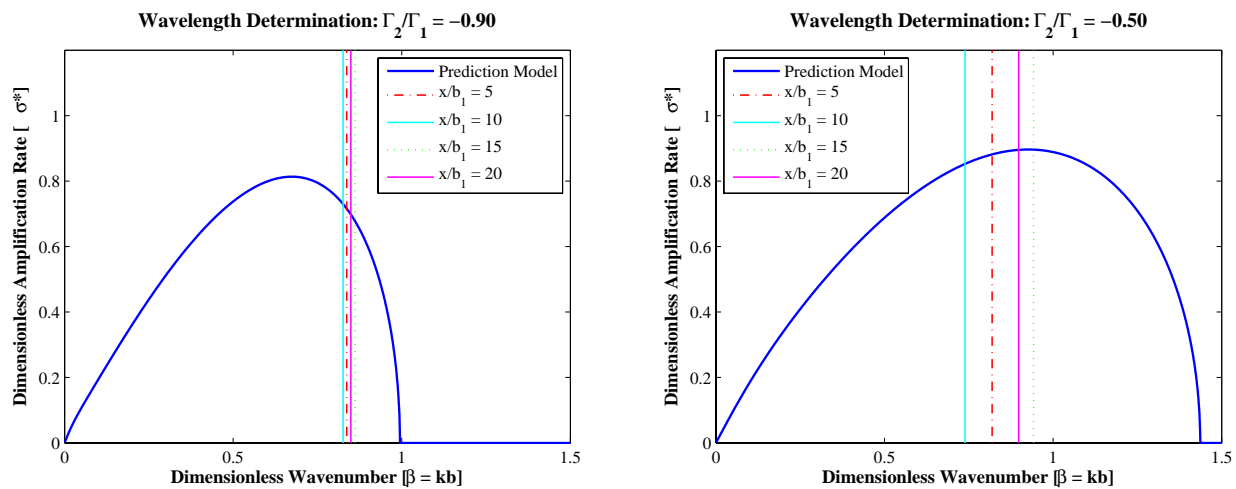


Fig. 4. Comparison of predicted wavelength for a rigidly-translating case (left) and a periodically-translating case (right)

The estimated wavelengths presented for the $\Gamma_2/\Gamma_1 = -0.50$, $b_2/b_1 = 0.45$ case in Figure 4 suggest that the wavelength of the resulting bending wave motion varies in the streamwise direction due to the periodic translation of the wake vortices. This result is not surprising as the effective vortex span is expected to vary periodically in the streamwise direction. The observed wavelengths are still consistent with the least stable wavenumbers from the instability model. Both results presented in Figure 4, strongly suggest that the bending wave motion is consistent with the expected behavior of the long-wavelength instability. These results further imply that the bending wavelength scales with the effective vortex span between the inboard and outboard vortices on each side of the wake centerline.

3.2 Examination of the Temporal Growth Rate

3.2.1 Amplitude Variation with Streamwise Location

Having captured images of several wake configurations at multiple streamwise stations, it was possible to use the image superimposition technique, described in section 2.3, to compare the temporal growth of the observed instability to that of the linearized model. Because the solution to the governing equations takes the form of $e^{\sigma t + ikx}$, where the temporal growth rate (σ) is scaled by the applied strain rate ($\varepsilon_i = \Gamma_j / 2\pi b^2$), it was possible to compare the measured wave amplitude to the analytical model. An axial perturbation (r_p) on the order of the effective core radius was assumed to trigger the instability at the least stable wavenumber. Thus, for a specific configuration, the amplitude of the unstable wave could be given by

$$A = |r_p| e^{\sigma t + ikx}, \quad (1)$$

where the time (t) is a function of the streamwise coordinate as the unstable wave is being convected at the free-stream velocity in the test section. The estimate of the core radius used for the axial perturbation was again obtained from the near-field hot-wire data. In the experiment, these perturbations are known to be attributed to free-stream turbulence.

The linear stability model was used to calculate the normalized growth rate ($\sigma^* = \sigma/\varepsilon$) for three configurations $\Gamma_2/\Gamma_1 = -0.90, -0.70$ and -0.50 with $b_2/b_1 = 0.45$, where the growth rate at the least stable wavenumber was used to predict amplitude variation in the streamwise coordinate. To obtain an amplitude estimate of the unstable outboard vortex using the theoretical model, the normalized growth rate was multiplied by the strain rate imposed by the inboard vortex. Owing to a relatively small sample size, the extrema on the error bars are given by the maximum and minimum amplitude values estimated in each group of images. The results presented in Figure 5 indicate that the temporal growth of the unstable wave is consistent with the exponential growth associated with the long-wavelength instability.

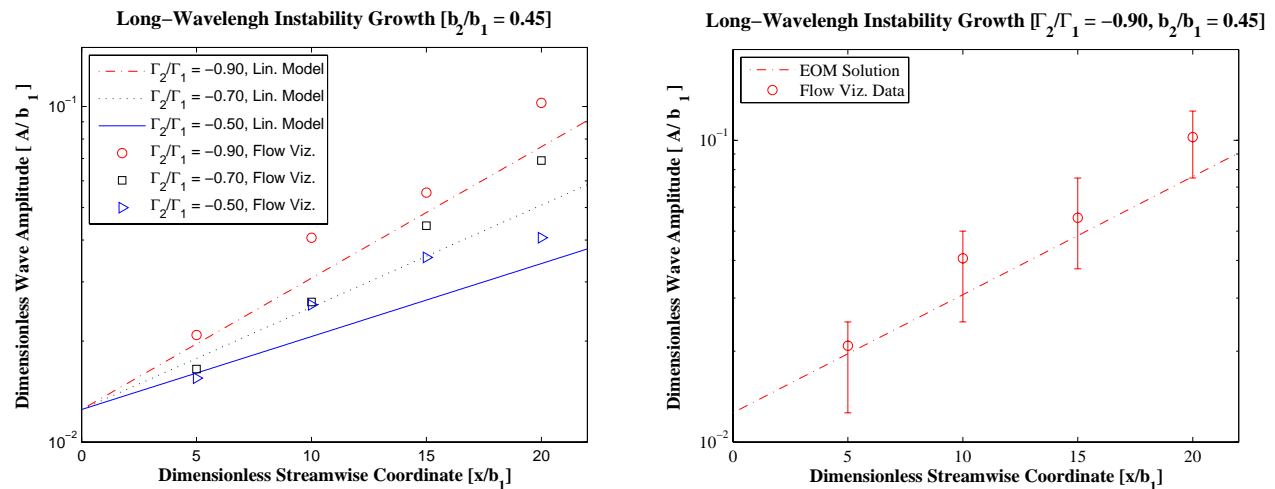


Fig. 5. Comparison of growth rates using both flow visualization estimations and linear stability theory for three highly-strained cases (left) and an estimation of error for the rigidly-translating case (right)

3.2.2. Amplitude Variation with Externally Applied Strain Rate

To further investigate the temporal growth behavior of the observed instability, the influence of the applied strain rate was investigated analytically and experimentally. Reiterating that the temporal growth rate is scaled by the externally applied strain rate in the linear stability model, it stands to reason that at any given streamwise location, the amplitude of an unstable wake vortex would be influenced by the applied strain rate. Furthermore recalling that the strain rate is a function of the circulation strength of the straining vortex, one would expect the amplitude of the unstable outboard vortex to vary with changes in the circulation strength of the inboard vortex. Equation 1 was again used as the analytical growth model for this comparison, although it is noted that the calculated growth rate varied with circulation strength, consistent with the solution of the eigenvalue problem.

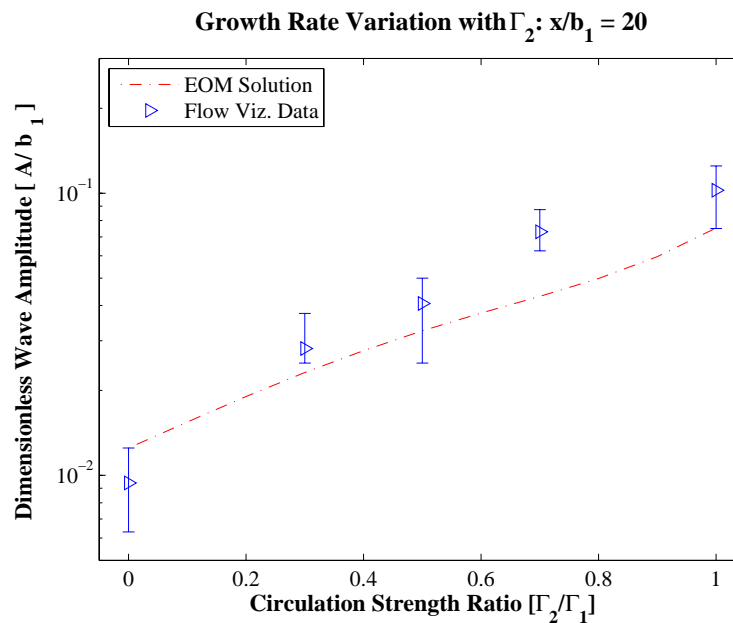


Fig. 6. Variation of temporal growth rate on a tip vortex with changes in the inboard flap vortex circulation strength

Examination of Figure 6 suggests that the amplitude of the unstable outboard vortex changes in a manner consistent with the variation of the applied strain rate. This result implies that the applied strain rate is an appropriate scaling for the temporal growth rate and that the velocity field induced by the flap vortex has the largest influence on the stability of the tip vortex. This is entirely consistent with the hypothesis that the observed motion is a long-wavelength instability dominated by the induced velocity field between a flap/tip vortex pair.

3.2.3 Bending Mode Symmetry and Plane Confinement

Referring to the model presented by Crow, one would expect the dominance of a symmetric instability mode. The symmetry of the long-wavelength mode suggests that the bending motion of each vortex within the unstable pair will exhibit symmetry across the center of the effective vortex span. Since it has been hypothesized that the unstable behavior observed during these experiments is a long-wavelength instability driven by the induced motion of the tip and flap vortices, one would expect to observe a symmetric bending behavior between these two vortices.

Inspection of Figure 7 clearly indicates the existence of symmetric motion within the tip/flap vortex pair. This behavior has been observed between the inboard and outboard vortices on both sides of the wake and appears to be most pronounced for highly strained configurations. The symmetric mode bending behavior serves to support the hypothesis that the observed behavior is a long-wavelength instability localized within the tip/flap vortex pair.

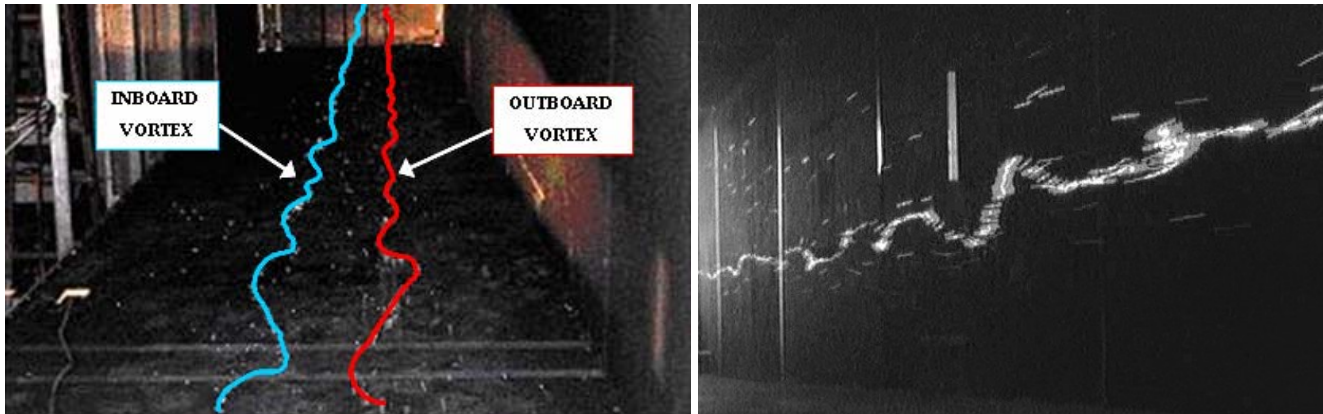


Fig. 7. Enhanced image of a tip/flap vortex pair (left) and an unstable outboard tip vortex (right). Both images suggest that the bending waves are confined to fixed planes.

By its analytical definition, the persistence of a long-wavelength instability implies that the bending wave behavior would be confined to inclined planes whose orientations are consistent with the principle strain directions. Analytically, these inclination angles are given by the eigenvector associated with the least stable eigenvalue mode. Examination of Figure 7 suggests that the perceived long-wavelength instability follows this trend. An identical matching of the analytical condition is not expected in the laboratory environment as the observed wake vortices are also influenced by two additional vortices within the flow field, the effects of the wind tunnel walls and the effects of turbulence and vortex wandering. Discrepancies between the analytical model and experiment may also be explained by the presence of an axial velocity component in the wake flow field, which has been neglected in the linear stability model. Having noted these potential sources of uncertainty, the results represented in Figure 7 are interpreted as entirely consistent with the persistence of a long-wavelength instability.

4 The Long-Wavelength Instability and Airport Capacity

In an effort to relate the experimentally achieved data to aircraft applications, the linear stability model was used to predict the time that is required for a tip/flap vortex pair to link. Noting the acceptable agreement of the flow visualization data with the predictive model, it seems plausible that the model could be used to predict the time required for the amplification of the unstable bending mode to amplify such that the two vortices in the pair would touch, or link. Under flight conditions, the vortex pair would form a series of vortex rings and would subsequently decay very rapidly. Recalling that the linearized eigenvalue solution yields a temporal growth rate where the associated eigenvector can be used to obtain the principle strain direction, and consequently the inclination angle of the confinement plane, it is possible to use Equation 1 to calculate the time required for the amplitude of the bending waves to touch. Such a calculation was completed for several rigidly-translating systems, whose

linking times are given in Figure 8. The cubic curve in Figure 8 denoting rigidly translating wake configurations is based upon the work of Rennich and Lele [12], where it was concluded that these configurations maintain the largest cross-flow strain rates throughout wake development.

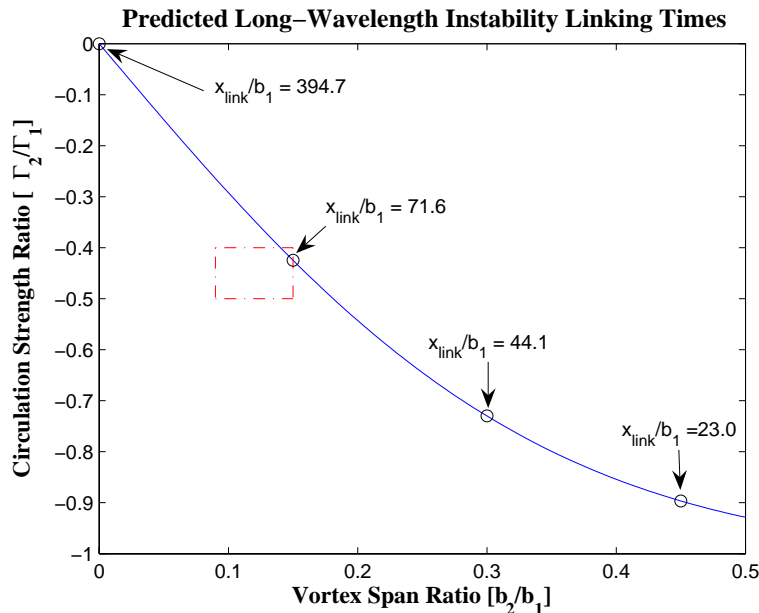


Fig. 8. Analytical prediction of the distance required for a linking of an unstable vortex pair. The red dashed box denotes wake configurations generated by current commercial aircraft.

When relating these predictions to airport capacity, it is useful to translate the results into aircraft variables. Assuming that a Boeing 747 has a wingspan near 200 ft (61 m), the required linking distance for a clean wing configuration, as shown in the upper-left corner of Figure 8, would be nearly 13 nautical miles in a calm atmosphere. In comparison, the most highly-strained configuration would require less than 1 nautical mile for a linking of the tip and flap vortices in a rigidly-translating wake. The data point representing current aircraft configurations implies that 2.34 nautical miles are necessary for a linking of the tip/flap vortex pair. It should be reiterated that these estimates are based on the linear stability model and do not take into account the effects of atmospheric turbulence or viscosity. These effects have been studied independently by Crow and Bate [13] while the effects of viscosity have been modeled by Iversen [14].

The measurements and predictions based on the visualization data clearly indicate that a rigidly-translating, four-vortex wake tends to break down following linking in a significantly shorter distance compared to that which is expected of a clean, two-wing configuration. The current analysis suggests that wake attenuation may be achieved by a proper wing span loading, resulting in a rigidly-translating system. Furthermore, these results suggest that wake attenuation may also be achieved by incorporating deployable vortex generating devices on the wing. Again, the ultimate goal of such passive control strategies is the maintenance of a sufficiently high rate of strain on each vortex for the support of large instability growth rates.

5 Summary and Conclusions

An experimental and analytical study into the stability of four-vortex wakes has been completed at the University of Notre Dame, with a portion of the flow visualization study having been presented in the current text. In the preceding sections, a novel approach to the experimental estimation of the amplitude and wavelength of a bending wave instability has been presented. The results of the flow visualization study, when compared with a linear stability model, clearly indicate that the observed bending wave motion is a manifestation of the long-wavelength instability that is primarily driven by the mutual interaction of a tip/flap vortex pair on each side of the wake centerline. Noting the agreement of the helium-bubble visualization data with the aforementioned linear stability model, it was possible to extend the linear model to make predictions regarding the time required for a breakdown of the hazardous wake structures. For a current aircraft configuration that yields a rigidly-translating wake, it has been shown that linking will occur in one-fifth of the distance required for that of a clean wing case. Such reductions in linking times may potentially result in the safe reduction in spacing between landing aircraft, yielding an increase in airport capacity.

References

1. Donaldson, C. duP., and Bilanin, A.J., *Vortex wakes of conventional aircraft*. AGARD Technical Report AG-204, NATO AGARD, 1975.
2. Crow, S.C., Stability theory for a pair of trailing vortices. *AIAA Journal*, Vol. 8, No. 12, pp. 2172-2179, 1970.
3. Saffman, P.G., *Vortex Dynamics*, Cambridge University Press, pp. 230-252, 1993.
4. Bristol, R.L., Ortega, J.M., Savas, O., On cooperative instabilities of parallel vortex pairs. *Journal of Fluid Mechanics*, Vol. 517, pp. 331-358, 2004.
5. Ortega, J.M., *Stability characteristics of counter-rotating vortex pairs in the wakes of triangular-flapped airfoils*. PhD dissertation, University of California at Berkeley, 1993.
6. McAlister, K.W. and Takahashi, R.K., *NACA 0015 wing pressure and trailing vortex measurements*. NASA Technical Report 3151, 1991.
7. Babie, B.M. and Nelson, R.C., Flow visualization study of far-field wake vortex interactions. *Proc. 11th International Symposium on Flow Visualization*, Paper No. 11ISFV-103, August 2004.
8. Nelson, R.C. and Babie, B.M., An experimental study of the stability of a four-vortex system. *Proc. 23rd AIAA Applied Aerodynamics Conference*, Paper No. 2005-4852, June 2005.
9. Babie, B.M. and Nelson, R.C., An experimental study of wake vortex instabilities, *Proc. 46th AIAA Aerospace Sciences Meeting & Exhibit*, Paper No. 2008-0363, January 2008.
10. Hale, R.W., Tan, P., Stowell, R.C., Iwan, L.S., Ordway, D.E., *Preliminary investigation of the role of the tip vortex in rotary wing aerodynamics through flow visualization*. Sage Action Inc. Technical Report SAI-RR-7402, 1974.
11. Eliason, B.G., Gartshore, I.S., Parkinson, G.V., Wind tunnel investigation of the Crow instability. *Journal of Aircraft*, Vol. 12, No. 12, pp. 985-988, 1975.
12. Rennich, S.C. and Lele, S.K., Method for accelerating the destruction of aircraft wake vortices. *Journal of Aircraft*, Vol. 36, No. 2, 1999.
13. Crow, S.C. and Bate, E.R., Lifespan of trailing vortices in a turbulent atmosphere. *Journal of Aircraft*, Vol. 13, No. 7, pp. 476-482, 1976.
14. Iversen, J.D., Correlation of turbulent trailing vortex data. *Journal of Aircraft*, Vol. 13, No. 5, pp. 338-342, 1976.

Copyright Statement

The authors confirm that they, and/or their company or institution, hold copyright on all of the original material included in their paper. They also confirm they have obtained permission, from the copyright holder of any third party material included in their paper, to publish it as part of their paper. The authors grant full permission for the publication and distribution of their paper as part of the ISFV13/FLUVISU12 proceedings or as individual off-prints from the proceedings.